AirborneWind Energy: Airfoil-Airmass Interaction

Mario Zanon, Sebastien Gros, Johan Meyers, Moritz Diehl

Preprints of the 19th World Congress
The International Federation of Automatic Control
Cape Town, South Africa. August 24-29, 2014

Airborne Wind Energy: Airfoil-Airmass Interaction

Mario Zanon * **Sébastien Gros** ** **Johan Meyers** *** **Moritz Diehl** ****

* *Electrical Engineering Department (ESAT-SCD) and Optimization in Engineering Center (OPTEC), KU Leuven, Kasteelpark Arenberg 10, B-3001 Leuven-Heverlee, Belgium (e-mail: mario.zanon@esat.kuleuven.be).*
** *Department of Signals and Systems, Chalmers University of Technology, Hörsalsvägen 11, SE-412 96 Göteborg, Sweden (e-mail: grosse@chalmers.se)*
*** *Department of Mechanical Engineering, KU Leuven, Celestijnenlaan 300 A, B3001 Leuven, Belgium (e-mail: johan.meyers@mech.kuleuven.be)*
**** *University of Freiburg - IMTEK, Georges-Koehler-Allee 102, 79110 Freiburg, Germany and * (e-mail: moritz.diehl@esat.kuleuven.be).*

Abstract: The Airborne Wind Energy paradigm proposes to generate energy by flying a tethered airfoil across the wind flow at a high velocity. While Airborne Wind Energy enables flight in higher-altitude, stronger wind layers, the extra drag generated by the tether motion imposes a significant limit to the overall system efficiency. To address this issue, two airfoils with a shared tether can reduce overall system drag. A study proposed in Zanon et al. (2013) confirms this claim by showing that, in the considered scenario, the dual-airfoil system is more advantageous than the single-airfoil one. The results computed in Zanon et al. (2013) however, do not model the interaction between the airfoils and the airmass. In this paper, the impact of the airfoil-airmass interaction on the extracted power is studied. As this phenomenon is complex to model, a blade element-momentum approach is proposed and the problem is solved by means of optimal control techniques.

1. INTRODUCTION

To overcome the major difficulties posed by the growing size and mass of conventional wind turbine generators Laks et al. (2009); Bossanyi (2005), the Airborne Wind Energy (AWE) paradigm proposes to eliminate the structural elements not directly involved in power generation. An emerging consensus recognizes crosswind flight as the most efficient approach to Airborne Wind Energy Loyd (1980). Crosswind flight extracts power from the airflow by flying an airfoil tethered to the ground at a high velocity across the wind direction. Power can be generated by (a) performing a cyclical variation of the tether length, together with cyclical variation of the tether tension or (b) by using on-board turbines, transmitting the power to the ground via the tether. In this paper, option (b) is considered, as investigated by e.g. *Makani Power* Makani Power (2006).

Because it involves a much lighter structure, a major advantage of power generation based on crosswind flight over conventional wind turbines is that higher altitude can be reached and a larger swept area be achieved, thereby reaching wind resources that cannot be tapped into by conventional wind turbines Diehl and Houska (2009).

⋆ This research was supported by Research Council KUL: PFV/10/002 Optimization in Engineering Center OPTEC, GOA/10/09 MaNet and GOA/10/11 Global real- time optimal control of autonomous robots and mechatronic systems. Flemish Government: IOF/KP/SCORES4CHEM, FWO: PhD/postdoc grants and projects: G.0320.08 (convex MPC), G.0377.09 (Mechatronics MPC); IWT: PhD Grants, projects: SBO LeCoPro; Belgian Federal Science Policy Office: IUAP P7 (DYSCO, Dynamical systems, control and optimization, 2012-2017); EU: FP7-EMBOCON (ICT-248940), FP7-SADCO (MC ITN-264735), ERC ST HIGHWIND (259 166), Eurostars SMART, ACCM.

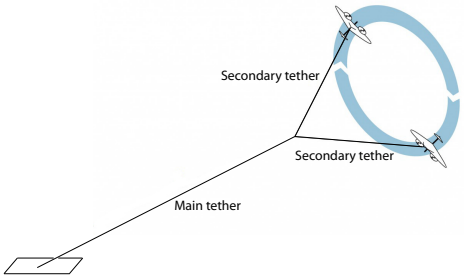

Fig. 1. Schematic of a dual-airfoil AWE system (from Payne and McCutchen (1976), Fig. 3).

Unfortunately, the drag due to the motion of the tether during crosswind flight has a significant impact on the system performance. To tackle this issue, the dual-airfoil design was first introduced in Payne and McCutchen (1976) and later investigated in e.g. Houska and Diehl (2007); Podgaets and Ockels (2006); Williams, P. and Lansdorp, B. and Ockels, W.J. (2008). The key idea of the dual-airfoil desing is to fly two airfoils connected on a single main tether (see Figure 1) in a balanced manner. As a result, only the shorter secondary tethers move at a high velocity and generate drag, while the motion of the main tether is negligible.

In order to fully exploit the gains of reducing the tether drag, the system and the planned trajectory must be carefully designed. In Zanon et al. (2013), a trajectory design method based on optimal control has been proposed to maximize the extracted power. This results in trajectories that a) balance the forces on the main tether, so as to minimize its motion, b) the generator

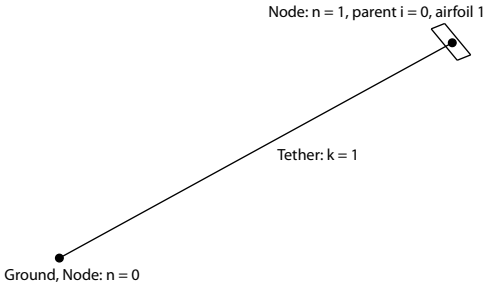

Fig. 2. Schematic of the single-airfoil architecture, with $N = 1$, $\mathcal{A} = \{1\}$, $T(1) = 0$.

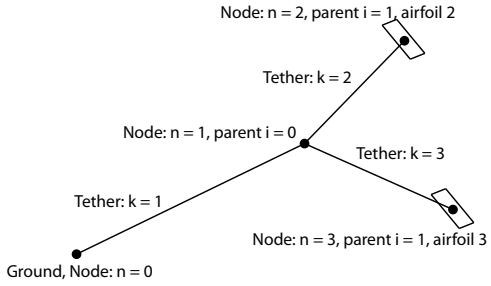

Fig. 3. Schematic of the dual-airfoil architecture, with $N = 3$, $\mathcal{A} = \{2,3\}$, $T(1) = 0$, $T(2) = 1$, $T(3) = 1$.

drag forces maximize the system efficiency, c) the tether lengths are chosen so as to achieve the best trade-off between reaching higher altitude and adding airborne mass, and d) the tether diameters must be selected so as to achieve the best trade-off between reducing the drag and withstanding the forces in the system.

The study proposed in Zanon et al. (2013) provides a comparison between single and dual airfoil systems for different airborne areas under the assumption of no interaction between the airfoils and the airmass, i.e. the presence of the airfoils does not reduce the velocity of the airmass. It is well known Manwell, J. F., McGowan, J. G. and Rogers, A. L. (2009); Bianchi, Fernando D. and Battista, Hernn de and Mantz, Ricardo J. (2007) that this hypothesis does not hold true for conventional wind turbines and the Betz law provides an upper bound to the energy that can be extracted from the airmass. Such analysis does not directly apply to AWE systems, and, to the authors' knowledge, no study is available in the literature, which considers interaction between the airfoil and the airmass. In this paper, the effect of such interaction is taken into account in the optimal control problem by introducing an interaction model which adapts the blade element-momentum theory to AWE systems.

This paper is organized as follows. First a multiple-airfoil model is proposed in Section 2. Section 3 describes the power-generation optimization problem, the solution approach used to compute power-generating trajectories, and the software used to perform the optimization. Section 4 proposes a comparison between optimal power generation based on single and dual airfoils for different approximations of the airfoil-airmass interaction. Finally, Section 5 concludes the paper and outlines further developments.

2. SYSTEM MODEL

The system is modeled following the procedure proposed in Zanon et al. (2013). Each airfoil has been modeled as a point mass and the tethers have been modeled with a finite element model. An orthonormal right-handed reference frame $e = \{e_x, e_y, e_z\}$ attached to the ground is chosen to generate the Cartesian coordinate system defining the positions of the airfoils. The frame e is chosen s.t. a) the wind is blowing in the e_x-direction, b) the vector e_z is opposed to the gravitational acceleration vector g. The origin of the coordinate system coincides with the attachment point of the main tether to the ground.

2.1 System Architecture

The system is described as a set of N nodes $n \in \{0,...,N\}$ with associated coordinate vectors $X_n \in \mathbb{R}^3$. The fixed node $X_0 = [0,\ 0,\ 0]^T$ stands for the attachment point of the AWE system to the ground. The subset $\mathcal{A} \subset \{1,...,N\}$ of the set of nodes describes the nodes associated to the airfoils. Assuming a tree structure, to each node $n \in \{1,...,N\}$ a single tether $k = n$ is associated, and the parent node i to which the tether is attached is defined by the map $i = T(n)$. See Figures 2 and 3 for an illustration. The system architecture is then defined by the number of nodes N, the set $\mathcal{A}$, and the map T. The proposed formulation allows for tree-like system architectures only.

In the following, the notation $X_n = [x_n, y_n, z_n]^T$ of the node coordinate vectors X_n is used. The position of the node n is given by $\mathcal{P}_n = x_n e_x + y_n e_y + z_n e_z$. Each tether $k = 1,...,N$ has associated length l_k and diameter d_k.

2.2 Airfoil model

For any node $n \in \{0,...,N\}$, we define the velocity relative to the airmass:

$$v_n = (\dot{x}_n - W)\, e_x + \dot{y}_n\, e_y + \dot{z}_n\, e_z,$$

where $W \in \mathbb{R}$ is the local wind velocity in the e_x direction. A generalization of this formulation to a 3D wind field is straightforward. If $n \in \mathcal{A}$, lift and drag forces act on the node. In the following formulas, C_{L}^n and C_{D}^n are the lift and drag coefficients of the airfoil, ρ is the air density and S the airfoil surface.

Introducing the roll angle ψ_i describing the tilting of the lift force around the axis v_n, the lift force can be defined by Zanon et al. (2013):

$$F_{\mathrm{L}}^n = \frac{1}{2}\rho S C_{\mathrm{L}}^n \left(\cos(\psi_i) f_L^n \|v_n\| - \sin(\psi_i) e_T^n \|v_n\|^2\right),$$
$$e_T^n = \frac{v_n \times e_r^n}{\|v_n \times e_r^n\|}, \qquad f_L^n = e_T^n \times v_n.$$

By definition F_{L}^n is always orthogonal to v_n, and lies in the plane defined by $\{e_r^n, v_n\}$ if $\psi_i = 0$.

The airfoil drag force is opposed to the relative velocity, and is readily given by:

$$F_{\mathrm{D}}^n = -\frac{1}{2}\rho S C_{\mathrm{D}}^n \|v_n\| v_n.$$

The drag generated by the onboard turbines can be modeled as:

$$F_G^n = -\kappa_n \|v_n\| v_n,$$

where $\dot{\kappa}_n(t) = u_{\kappa_n(t)}$, $u_{\kappa_n(t)}$ is a control variable and we assume that the generated force is opposed to the relative velocity. The resulting aerodynamic power is:

$$P_n = v_n^T F_G^n = -\kappa_n \|v_n\|^3.$$

The resulting airfoil aerodynamic force acting on airfoil n is given by $F_{\mathrm{A}}^n = F_{\mathrm{L}}^n + F_{\mathrm{D}}^n + F_G^n$.

In this model, it is assumed that the time-derivative of the lift coefficient is directly controlled, and the drag coefficient C_{D}^n is approximated by Pamadi (2003); Cook (2007): $C_{\mathrm{D}}^n = C_{\mathrm{D}}^0 + C_{\mathrm{D}}^I (C_{\mathrm{L}}^n)^2$, where C_{D}^0 and C_{D}^I are the airfoil drag and induced-drag coefficients respectively.

The kinetic and potential energy functions associated with the airfoil dynamics are:

$$\mathcal{T}_{\mathrm{A}}^n = \frac{1}{2} M_{\mathrm{A}} \|\dot{X}_n\|^2, \quad \mathcal{V}_{\mathrm{A}}^n = M_{\mathrm{A}} g z_n,$$

where M_{A} is the airfoil mass, and the Lagrange function for the airfoils reads:

$$\mathcal{L}_{\mathrm{A}} = \mathcal{T}_{\mathrm{A}} - \mathcal{V}_{\mathrm{A}}, \quad \mathcal{T}_{\mathrm{A}} = \sum_{n \in \mathcal{A}} \mathcal{T}_{\mathrm{A}}^n, \quad \mathcal{V}_{\mathrm{A}} = \sum_{n \in \mathcal{A}} \mathcal{V}_{\mathrm{A}}^n.$$

2.3 Wind and atmosphere model

Assuming a laminar wind flow with a logarithmic wind shear model blowing uniformly in the e_x-direction, the free-flow windspeed W_∞ at altitude z is given by Manwell, J. F., McGowan, J. G. and Rogers, A. L. (2009):

$$W_\infty(z) = W_0 \frac{\log(z/z_{\mathrm{r}})}{\log(z_0/z_{\mathrm{r}})}, \tag{1}$$

where $W_0 \in \mathbb{R}$ is the wind velocity at altitude z_0 and z_r is the ground roughness.

To account for the drop of density with altitude the following atmospheric model is introduced Andrews (2010):

$$T(z) = T_0 - T_L z, \quad P(z) = P_0 \left(1 - \frac{T_L z}{T_0}\right)^{\frac{gM_a}{RT_L}}, \quad \rho(z) = \frac{PM_a}{RT},$$

where T_0 is the sea level standard temperature, T_L is the temperature lapse rate, P_0 is the pressure at sea level, M_a is the molar air density and R is the universal gas constant.

2.4 Tether model

In the proposed formulation, the tethers are modeled with a lumped mass Finite Element Model. For a rigid tether $k \in \{1,...,N\}$ of length l_k, density ρ_c, diameter d_k, we define N_k elements linked by massless rigid links, where link k,j connects elements k,j and $k,j+1$. Note that with this notation, the position of the endpoint X_{k,N_k} of each tether k coincides with the position X_k of node k. In the proposed model, all links have the same length $l_{k,j} = l_k/N_k$ and each element k,j with $1 < j < N_k$ has mass $m_{k,j} = m_k/(N_k+1)$, while $m_{k,0} = mk, N_k = m_k/(2(N_k+1))$. The tether kinetic and potential energy functions read:

$$\mathcal{T}_{\mathrm{T}}^k = \sum_{j=1}^{N_k} \frac{1}{2} m_{k,j} \|\dot{X}_{k,j}\|^2, \qquad \mathcal{V}_{\mathrm{T}}^k = \sum_{j=1}^{N_k} m_{k,j} g z_{k,j},$$

where $m_{k,j}$ is the mass associated with each element and $\dot{X}_{k,j}$ and $z_{k,j}$ are respectively its velocity and height.

The tether drag on each tether section k,j is given by:

$$F_S^{k,j} = -\frac{1}{2} \rho_{k,j} d_k l_{k,j} C_{\mathrm{T}} \|v_{k,j}\| v_{k,j},$$

where C_{T} is the drag coefficient of a cylinder, $l_{k,j}$ is the length of link k,j and $v_{k,j}$ is the velocity of its midpoint, computed as

$$v_{k,j} = W\left(\frac{z_{k,j} + z_{k,j+1}}{2}\right) + \frac{\dot{X}_{k,j} + \dot{X}_{k,j+1}}{2},$$

where W is the windspeed at the midpoint's altitude. The lift generated by the tethers is not considered in this formulation. The contribution of the tether drags to the generalized forces acting on the generalized coordinates $X_{k,j}$ is given by:

$$F_T^{k,j} = \frac{F_S^{k,j} + F_S^{k,j+1}}{2}.$$

2.5 Generalized forces

The vector of generalized forces $F = \left[F_{1,1}^T, ..., F_{N,N_N}^T\right]^T$, where $F_{k,j} \in \mathbb{R}^3$ is the vector of generalized forces acting on the vector of generalized coordinates $X_{k,j}$, is resulting from the sum of the various contributions coming from tether drags and airfoil aerodynamic forces. Though this summation can be performed very intuitively, it can be formulated as the following systematic construction. For any $k \in \{1,...,N\}, j \in \{1,...,N_k\}$, $F_{k,j}$ is given by:

$$F_{k,j} = \begin{cases} F_T^{k,j} & \text{if } j \in 1,...,N_k - 1 \\ F_T^{k,j} + \sum F_T^{k_c,0} & \text{if } T(k_c) = k \text{ and } j = N_k \\ F_T^{k,j} + F_{\mathrm{A}}^k & \text{if } k \in A \text{ and } j = N_k \end{cases}$$

2.6 System model

In the following, the generalized coordinate vector $X = \left[X_{1,1}^T, ..., X_{N,N_N}^T\right]^T$ of the system is used. The system is considered as a set of independent tethers and airfoils, with associated Lagrange functions. The tethers introduce a set of constraints in the system configuration, given by:

$$G_{k,j} = \frac{1}{2}\left((X_{k,j+1} - X_{k,j})^T (X_{k,j+1} - X_{k,j}) - l_{k,j}^2\right) = 0, \tag{2}$$

for $k = 1,...,N$, $j = 1,...,N_k$. The system Lagrange function reads:

$$\mathcal{L} = \mathcal{T} - \mathcal{V} - \lambda^T G, \quad \mathcal{T} = \mathcal{T}_{\mathrm{A}} + \mathcal{T}_{\mathrm{T}}, \quad \mathcal{V} = \mathcal{V}_{\mathrm{A}} + \mathcal{V}_{\mathrm{T}},$$

where $\lambda \in \mathbb{R}^K$ is the vector of Lagrange multipliers associated to the constraints G. Using the Lagrange equation de Jalón, J. G. and Bayo, E. (1994) $\frac{d}{dt}\frac{\partial \mathcal{L}}{\partial \dot{X}} - \frac{\partial \mathcal{L}}{\partial X} = F$, it can be verified that the system dynamics are given by the following index-3 DAEs:

$$\mathcal{T}_{\dot{X}\dot{X}} \ddot{X} + G_X^T \lambda + \mathcal{V}_X = F, \qquad G = 0, \tag{3}$$

where λ is the DAE algebraic state, $G_X = \frac{\partial G}{\partial X}$, $\mathcal{T}_{\dot{X}\dot{X}} = \frac{\partial^2 \mathcal{T}}{\partial \dot{X}^2}$ and $\mathcal{V}_X = \frac{\partial \mathcal{V}}{\partial X}$.

For any $t_0 \in \mathbb{R}$, equation (3) can be reformulated as an index-1 DAE by performing index reduction, which yields $\ddot{G}(t) = 0, \dot{G}(t_0) = 0, G(t_0) = 0$. The resulting equations read (together with the consistency conditions):

$$\begin{bmatrix} \mathcal{T}_{\dot{X}\dot{X}} & G_X^T \\ G_X & 0 \end{bmatrix} \begin{bmatrix} \ddot{X} \\ \lambda \end{bmatrix} = \begin{bmatrix} F - \mathcal{V}_X \\ -\dfrac{\partial}{\partial X}\left(G_X \dot{X}\right) \dot{X} \end{bmatrix}, \tag{4}$$

$$G(t_0) = 0, \qquad \dot{G}(t_0) = \left(G_X \dot{X}\right)_{t=t_0} = 0. \tag{5}$$

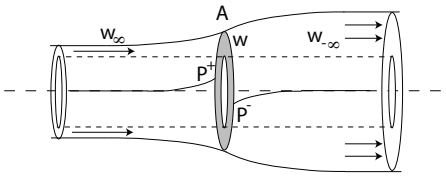

Fig. 4. Schematic of the airflow through an actuator disk (grey area) of area A. W_∞ is the free flow velocity, W the flow velocity at the actuator disk, $W_{-\infty}$ the velocity after the actuator disk. P^+ and P^- stand for the pressure just before and after the actuator disk.

It can be verified that the tension in tether k is readily given by:

$$\Gamma_k = \lambda_k l_k.$$

2.7 Blade-Element–Momentum Theory for AWE Systems

The blade-element–momentum (BEM) theory for conventional wind turbines considers the interaction between a blade element and the airflow. The main assumption is that, given the annulus swept by the considered blade element, the change of momentum of the air which passes through it is due only to the force exerced by the blade element on the airmass Burton, T., Sharpe, D., Jenkins, N. and Bossanyi, E. (2001).

In the following, the BEM theory is formulated for AWE systems. Note that, in this case, no analytic solution can be computed, as the annulus swept by the AWE system depends on the trajectory flown by the airfoil. The derivation will thus be included in the optimization problem as a constraint which bounds the maximum power that the system can extract from the air mass by adapting the wind velocity at the swept annulus.

As shown in Figure 4, the wind field velocity $W(z)$ at the swept annulus is less than the free flow velocity $W_\infty(z)$, and depends on the average thrust F_D exerted on the air mass by the actuator disk. This effect is conventionally represented by the axial induction factor a, defined through $W \equiv (1-a)W_\infty$, $0 < a < 1$.

The change of air mass momentum in the annular control volume (cf. Figure 4) results from the thrust force F_D acting on the annulus, such that

$$F_D = \rho A W \left(W_\infty - W_{-\infty}\right), \tag{6}$$

where $W_{-\infty}$ is the steady-state flow velocity in the far wake of the annulus (see Figure 4). Locally around the annular actuator disk, we can further express (since the velocity is continuous over the disk)

$$F_D = A\left(P^+ - P^-\right), \tag{7}$$

such that the difference of pressure on the annulus is given by

$$P^+ - P^- = \rho W \left(W_\infty - W_{-\infty}\right). \tag{8}$$

From Bernoulli's principle, the conservation of the air mass energy along streamlines before and after the actuator disk requires that

$$\frac{1}{2}\rho W^2 + P^+ = \frac{1}{2}\rho W_\infty^2 + P_0,$$
$$\frac{1}{2}\rho W^2 + P^- = \frac{1}{2}\rho W_{-\infty}^2 + P_0,$$

where P_0 is the pressure in the free flow, resulting in

$$P^+ - P^- = \frac{1}{2}\rho\left(W_\infty^2 - W_{-\infty}^2\right). \tag{9}$$

By combining (8) and (9), it can be verified that

$$W_{-\infty} = 2W - W_\infty = (1-2a)W_\infty. \tag{10}$$

Using (6) and (10), the power extracted from the flow at is then given by:

$$P_D(a) = F_D W = 2\rho A a (1-a)^2 W_\infty^3. \tag{11}$$

This result is essentially the same as the classical Betz result for wind turbines (albeit there for a circular area instead of an annulus). The Betz limit occurs for $a = 1/3$, leading to a power coefficient $C_p \equiv P/(\rho W_\infty^3/2) = 16/27$, but this presumes an ideal case with frictionless power extraction. In the context of an AWE system, drag forces on the wing, an the possibility to fly the wing at different radii R and speeds, leads to an optimization problem in which $a = 1/3$ will not be recovered as an optimum.

For an AWE system, P_D is also given by summing up all the average power dissipated by the system P_E, i.e. the total average power resulting from the drag yielded by the tether, airfoil and turbines:

$$P_D = P_E = \frac{1}{T_p}\int_0^{T_p}\left(\sum_{i\in\mathcal{A}}\left(P_i + v_i^T F_{\mathrm{D}}^i\right) + \sum_{n=1}^{N} v_n^T F_T^n\right)dt. \tag{12}$$

Variable P_E depends on the wind field velocity $W(z)$, taken as $W(z) = (1-a)W_\infty(z)$ in this paper. As a result, within Betz' framework the implicit equality:

$$P_D(a) = P_E\left((1-a)W_\infty\right), \tag{13}$$

must hold for some value of a. In the framework of optimal control a is treated as a decision variable and the implicit relationship (13) as an equality constraint.

Because of the wind shear, the wind velocity on the annulus swept by the AWE system is not uniform, hence it is proposed here to evaluate (11) using the integral:

$$P_D(a) = 2\rho a(1-a)^2\int_A W_\infty^3 dA. \tag{14}$$

It can be verified that for a single airfoil, P_D can be computed using:

$$P_D(a) = 2\rho a(1-a)^2\int_0^{T_p} z_{\mathrm{tip}}\dot{y}_{\mathrm{tip}} W_\infty(z_{\mathrm{tip}})^3 dt, \tag{15}$$

where the coordinate vector $X_{\mathrm{tip}} = \begin{bmatrix} x_{\mathrm{tip}} & y_{\mathrm{tip}} & z_{\mathrm{tip}}\end{bmatrix}^T$ is the airfoil outer-tip position in frame e. For airfoil $n \in \mathcal{A}$, X_{tip}^n is given by:

$$X_{\mathrm{tip}}^n = \frac{A_{\mathrm{R}}}{2S}\left(\sin(\psi_i) f_L^n \|v_n\|^{-1} + \cos(\psi_i) e_T^n\right),$$

where A_{R} is the airfoil aspect ratio, and $w_s = A_{\mathrm{R}}/S$ is the airfoil wingspan. For dual-airfoil systems, both airfoils fly the same trajectories, and the area A can be computed based on the trajectory of any of the two airfoils.

2.8 Model assumptions & discussion

The proposed model is based on the following assumptions:

(1) the tethers are modelled with a lumped-mass finite element model
(2) the lift forces are orthogonal to the airfoil transversal axis
(3) the airfoils have a perfect yaw control, resulting in no sideslip
(4) the time-derivatives of the lift coefficient and roll angle are controlled and actuation is instantaneous
(5) the airfoil-airmass interaction is modeled with a blade element-momentum approach

The proposed model construction can straightforwardly accommodate a 6-DOF airfoil description (including the rotational dynamics) and more elaborate aerodynamic models. Yet in this paper a simple model was preferred, so as to reduce the complexity of the presentation.

The proposed framework for taking into account the interaction between the airfoils and the airmass involves a rather simple formulation and can fail to accurately capture all aerodynamic phenomena, yet, it allows to introduce a model of the interaction in the optimization problem. The improvement of the airfoil-airmass interaction model is the subject of ongoing research.

3. OPTIMIZATION PROBLEM

The airfoil trajectories as well as the tether lengths and sections are manipulated so as to maximize the system average power generation over an orbit of free duration T_p. The periodicity of the system is guaranteed by satisfying the boundary conditions:

$$Z^T(X(0) - X(T_p)) = 0, \tag{16}$$

where matrix Z is introduced to satisfy the Linear Independence Constraint Qualification (LICQ) Zanon et al. (2013).

In order to ensure that the tethers are always under tension but that their resistance is never exceeded, the constraints:

$$\frac{\gamma}{f_s}\frac{\pi}{4}d_k^2 \geq \Gamma_k(t) = \lambda_k l_k \geq 0, \quad \forall t, k = 1,...,N, \tag{17}$$

are imposed, where γ is the tether yield strength and f_s the safety factor. Moreover, the following bounds are proposed:

$$\begin{aligned} 0 \leq C_{\mathrm{L}}^i \leq 1, \qquad & -5\ \mathrm{s}^{-1} \leq \dot{C}_{\mathrm{L}}^i \leq 5\ \mathrm{s}^{-1}, \\ -80^\circ \leq \psi_L^i \leq 80^\circ, \qquad & -5\ \mathrm{s}^{-1} \leq \dot{\psi}_L^i \leq 5\ \mathrm{s}^{-1}, \\ -1000\ \mathrm{kg/(ms)} \leq \dot{\kappa}_i \leq 1000\ \mathrm{kg/(ms)}, & \quad \forall t, i \in \mathcal{A}. \end{aligned} \tag{18}$$

The periodic power optimization problem reads:

$$\begin{aligned} \bar{P} = \max_{U,X,\theta,a,T_p} \ & \frac{1}{T_p}\int_0^{T_p} \sum_{i\in\mathcal{A}} P_i dt, \\ s.t.\ & (4)-(5),(13),(16)-(18) \end{aligned} \tag{19}$$

where $U_i = \{\dot{C}_{\mathrm{L}}^i,\ \dot{\psi}_L^i,\ \kappa_i\},\ i \in \mathcal{A},\ \theta_k = \{l_k,\ d_k\},\ k = 1,...,N$. Note that T_p is an optimization variable, thus the duration of the orbit will be adapted by the optimizer so as to maximize the average power. In order to be able to treat this problem, a time transformation is introduced (Diehl, 2001, p. 27).

For the dual airfoils the additional constraint $\|X_2 - X_3\|^2 \geq w_s^2$ ensures that no collision occurs between the airfoils. Such a constraint is though never active for an optimal trajectory.

3.1 Solution approach

The Optimal Control Problem (19) is large-scale and highly non-convex and therefore requires a good initial guess to be tackled by derivative-based optimization. However, no such guess is readily available. To address this issue, a complex procedure is needed to compute an initial guess for problem (19).

For the dual-airfoil system, solving (19) on a full orbit yields quasi-identical trajectories for the two airfoils, hence (19) was solved on a half orbit instead, using the periodicity conditions $X_2(0) = X_3(\frac{1}{2}T_p), X_3(0) = X_2(\frac{1}{2}T_p)$ so as to match the terminal state of one airfoil with the initial state of the other. For both the single and dual-airfoil problems, the control input profiles were discretized using a piecewise-constant parametrization having 20 intervals per full orbit. One collocation element has been used per control interval.

3.2 Methods & Software

Because dynamics (4) are unstable, a simultaneous optimal control technique is required to optimize the system model. In this paper, the discretization of the model dynamics (4) was based on a direct collocation approach Biegler (2010), where the model simulation, constraints and optimization are handled simultaneously in a large-scale sparse Nonlinear Program (NLP). Collocation approaches provide a straightforward way to deal with implicit index-1 DAE systems Biegler (2010).

The problem transcription was performed using the open-source optimization framework *CasADi* Andersson et al. (2012). The resulting NLP was solved using the interior-point solver *IPOPT 3.10.1* Wächter and Biegler (2006) using *WSMP* as a linear solver.

4. NUMERICAL RESULTS

The parametric study aims at assessing what is the impact of the airfoil-airmass interaction on the extracted power by means of optimization. In particular, it is of most interest to assess if including a model of this interaction with the airmass (see Section 2.7) makes the single airfoil more advantageous than the dual.

The study was based on airfoils having a maximum gliding ratio $L/D = 25$. The tethers are assumed to be made of *Dyneema®*, which has a very high stiffness and yield strength for a low density. The fixed model parameters can be found in Zanon et al. (2013). For the single airfoil the tether has been discretized using 5 segments. For the dual airfoils the main tether has been discretized using 20 segments, while 5 segments were used for both secondary tethers. This results in 41 states for the single airfoil and 207 states for the dual airfoils.

Using the method proposed in Section 3.1, a solution to (19) for the single-airfoil system using parameter values $S = 500\ \mathrm{m}^2$ and $M_A/S = 20\ \mathrm{kg/m}^2$, and a solution for the dual-airfoil system using parameter values $S = 250\ \mathrm{m}^2$ and $M_A/S = 20\ \mathrm{kg/m}^2$ are computed. The choice of using large-scale systems stems from the results computed in Zanon et al. (2013). The biggest studied system is the one for which dual airfoils are less advantageous, thus the one for which the single airfoil is most competitive.

The computed trajectories for the dual and single airfoil are displayed in Figure 5. It can be seen that the dual airfoils fly

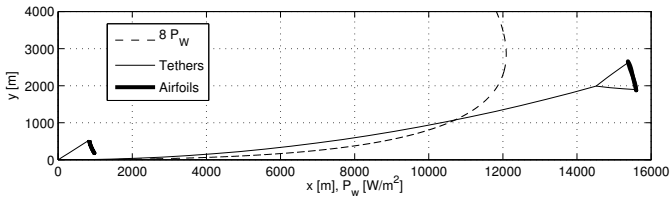

Fig. 5. Comparison between the optimal trajectories of the single and dual airfoils for a total wing surface $S_{\text{tot}} = 500\,\text{m}^2$. The trajectories are shown as thick lines. The available wind power $P_w = \rho W_\infty^3/2$ is plotted as a dashed line.

at a much higher altitude and at much longer tether lengths than the single airfoil. The trajectories obtained in this study are comparable to the ones obtained in Zanon et al. (2013). The trajectory of each airfoil is smooth and almost circular.

The most noticeable difference from the study proposed in Zanon et al. (2013) can be seen in the power extracted from the airmass. In Figure 6 the average power extracted by the single and dual airfoil systems is compared. Two cases are considered: a) the airfoil-airmass interaction is modeled and b) the interaction is not modeled. In both cases, the dual airfoils are more advantageous, but it can be seen that the airfoil-airmass interaction has a stronger impact on the dual airfoils. As it can be seen from Figure 6, the dual airfoils extract 39% less power when the airfoil-airmass interaction is modeled, while the power drop for the single airfoil is 27%.

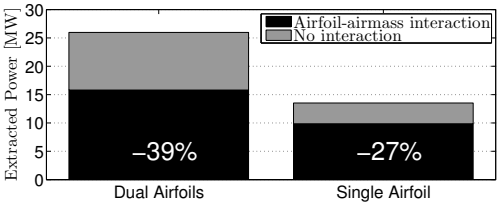

Fig. 6. Dual vs. one large single airfoil: average power output with and without consideering the airfoil-airmass interaction.

5. CONCLUSION & FURTHER DEVELOPMENTS

This paper has proposed a refinement of the results obtained in Zanon et al. (2013). An airfoil-airmass interaction model has been proposed, in order to investigate if the dual airfoils are indeed more advantageous then the single airfoil.

The results show that the power drop due to the interaction with the airmass is higher for the dual airfoil system. Nevertheless, the dual airfoils still extract more power than the single airfoil.

More elaborate models of the interaction between the airfoil and the airmass are the subject of ongoing research.

REFERENCES

Andersson, J., Åkesson, J., and Diehl, M. (2012). CasADi – A symbolic package for automatic differentiation and optimal control. In S. Forth, P. Hovland, E. Phipps, J. Utke, and A. Walther (eds.), *Recent Advances in Algorithmic Differentiation*, Lecture Notes in Computational Science and Engineering. Springer, Berlin.

Andrews, D. (2010). *An Introduction to ATMOSPHERE PHYSICS*. Cambridge University Press.

Bianchi, Fernando D. and Battista, Hernn de and Mantz, Ricardo J. (2007). *Wind Turbine Control Systems*. Springer.

Biegler, L.T. (2010). *Nonlinear Programming*. MOS-SIAM Series on Optimization. SIAM.

Bossanyi, E.A. (2005). Further Load Reductions with Individual Pitch Control. *Wind Energy*, 8, 481–485.

Burton, T., Sharpe, D., Jenkins, N. and Bossanyi, E. (2001). *Wind Energy Handbook*. John Wiley and Sons, Ltd, Chichester, UK.

Cook, M.V. (2007). *Flight Dynamics Principles*. Elsevier Science.

de Jalón, J. G. and Bayo, E. (1994). *Kinematic and Dynamic Simulation of Multibody Systems: The Real-Time Challenge*. Springer-Verlag.

Diehl, M. (2001). *Real-Time Optimization for Large Scale Nonlinear Processes*. Ph.D. thesis, Universität Heidelberg.

Diehl, M. and Houska, B. (2009). Windenergienutzung mit schnell fliegenden Flugdrachen: eine Herausforderung für die Optimierung und Regelung - Wind Power via Fast Flying Kites: a Challenge for Optimization and Control. *at-automatisierungstechnik*, 57(10), 525–533. doi: 10.1524/auto.2009.0798.

Houska, B. and Diehl, M. (2007). Optimal Control for Power Generating Kites. In *Proc. 9th European Control Conference*, 3560–3567. Kos, Greece,. (CD-ROM).

Laks, J., Pao, L., and Wright, A. (2009). Control of Wind Turbines: Past, Present, and Future. In *American Control Conference*, 2096–2103.

Loyd, M. (1980). Crosswind Kite Power. *Journal of Energy*, 4(3), 106–111.

Makani Power (2006). Makani Power Homepage. http://www.makanipower.com/.

Manwell, J. F., McGowan, J. G. and Rogers, A. L. (2009). *Wind Energy Explained: Theory, Design and Application, Second Edition*. John Wiley & Sons, Ltd, Chichester, UK.

Pamadi (2003). *Performance, Stability, Dynamics, and Control of Airplanes*. American Institute of Aeronautics and Astronautics, Inc.

Payne, P. and McCutchen, C. (1976). Self-Erecting Windmill. United States Patent 3987987.

Podgaets, A. and Ockels, W. (2006). Flight control and stability of a multiple kites tethered system. In *Proceedings of Renewable Energy Conference*.

Wächter, A. and Biegler, L. (2006). On the Implementation of a Primal-Dual Interior Point Filter Line Search Algorithm for Large-Scale Nonlinear Programming. *Mathematical Programming*, 106(1), 25–57.

Williams, P. and Lansdorp, B. and Ockels, W.J. (2008). Modeling of Optimal Power Generation using Multiple Kites. In *AIAA Modelling and Simulation Technologies Conference and Exhibit, Honolulu, Hawaii, USA*.

Zanon, M., Gros, S., Andersson, J., and Diehl, M. (2013). Airborne Wind Energy Based on Dual Airfoils. *IEEE Transactions on Control Systems Technology*, 21.